Appl. Phys. B (2017) 123:245
DOI 10.1007/s00340-017-6814-8

Applied Physics B
Lasers and Optics

An open-path tunable diode laser absorption spectrometer for detection of carbon dioxide at the Bonanza Creek Long-Term Ecological Research Site near Fairbanks, Alaska

D. Michelle Bailey[1] · Erin M. Adkins[1] · J. Houston Miller[1]

Received: 31 January 2017 / Accepted: 14 August 2017 / Published online: 6 September 2017

Abstract We have developed a low-power, open-path, near-infrared (NIR) tunable diode laser sensor for the measurement of near ground-level concentrations of greenhouse gases. Here, we report on instrument design, characterization, and initial measurements of carbon dioxide concentrations during deployment to a thermokarst collapse scar bog near Fairbanks, AK (USA). The optics "launch-box" portion of the instrument couples radiation from an NIR, distributed feedback diode laser operating near 1572 nm with a visible laser for alignment purposes. The outgoing beam is directed through a 3.2-mm hole in a parabolic mirror and the launch-box is oriented using a two axis, altitude-azimuth telescope mount such that the beam strikes a retroreflector target at a set distance downfield. The beam then retraces the path back to the launch-box where the light is collected on the surface of the parabolic mirror and focused onto a multimode fiber that transfers the radiation to an InGaAs detector. Sweeps over a ~1.6 cm^{-1} spectral region were collected at a rate of 500 scans per second and were typically stored as 10 s sweep averages. These averaged sweeps could be individually spectrally fit for CO_2 concentration or averaged into a single spectrum for fitting (after correction for slight frequency drift). Field data reported here was averaged for 2.5 min and was found to follow trends in diurnal cycles of CO_2 concentration cycles reported by sensors located nearby in the field site.

This article is part of the topical collection "Field Laser Applications in Industry and Research" guest edited by Francesco D'Amato, Erik Kerstel, and Alan Fried.

✉ J. Houston Miller
houston@gwu.edu

[1] George Washington University, 800 22nd Street NW, Washington, DC 20052, USA

1 Introduction

The addition of carbon to the atmosphere through anthropogenic emissions of greenhouse gases (GHGs) and the subsequent impact on global climate may be the most important environmental issue facing the planet. Two of the most critical greenhouse gases, carbon dioxide (CO_2) and methane (CH_4), constitute 76 and 16%, respectively, of anthropogenic emissions in 2010 [1]. Because models predict the potential for dramatic and irreversible changes in global climate with a 2.0 °C increase in global surface temperature compared to pre-industrial levels [2], emission reductions of these and other GHGs have been recommended and agreed upon in the Copenhagen accord [2, 3]. Therefore, as efforts to reduce emissions carry on, it is imperative to continue monitoring concentrations of critical gases on both local and global scales.

Advances in remote sensing have led to the ability to collect large-scale datasets in a relatively short period of time. Current missions include GOSAT, a satellite operated by the Japanese Aerospace Exploration Agency (JAXA) for measurement of CO_2 and CH_4 in the atmospheric column, and OCO-2, led by the National Aeronautics and Space Administration (NASA) with a focus on CO_2 column concentrations. GOSAT transverses the globe on a 3-daytime scale with maximum spatial resolution, or field-of-view (FOV) for the Fourier Transform Spectrometer, of 10.5 km [4]. Upon initial deployment, OCO-2 operated on a 16-day global observation cycle [5] and can collect measurements with as low as 3 km^2 spatial scale [6]. Both missions utilize light reflected from the surface of the Earth to measure column concentrations [4–6]. This type of measurement can allow for interferences from clouds, aerosols, or rough terrain on Earth's surface. Although methods exist for determining contamination-free data, such as measuring molecular

oxygen, one example for OCO-2 [5], or the use of the Cloud and Aerosol Imager for GOSAT [4], both instruments benefit from the use of ground-based or other in situ measurements for validation [5–8].

The primary ground-based network used for validation of remote sensing instruments is the Total Column Carbon Observing Network (TCCON). Each TCCON site is equipped with a high-resolution, sun-looking Fourier transform spectrometer for measurement of CO_2, CH_4, and a variety of other species in the atmospheric column [9]. The benefits of TCCON are offset by the high-cost of each installation thus limiting the network's spatial distribution. In an effort to increase spatial coverage of near-surface GHG measurements, campaigns using aircraft or mobile laboratories are common [10–13]. Although more insight into spatial distribution can be achieved with these methods, limitations remain with respect to location of campaigns, the potential for replicate measurements, and the time-span available to investigate seasonal variability. Open-path spectroscopy offers the potential for measurements that are both temporally and spatially resolved that can further contribute to validation of remote sensing products.

In addition to the introduction of carbon to the atmosphere from anthropogenic emissions is the increase in atmospheric carbon from natural feedbacks from sources such as thawing permafrost, as global temperatures continue to increase [14]. Permafrost is formally defined as soil (which often has substantial water content) that is continuously frozen for 24 consecutive months [15, 16]. Approximately, 25% of the Earth's terrestrial surface is underlain by these soils which have depths ranging from a few centimeters to several meters and that are separated from the atmosphere by an "active layer" which is often rich in carbon [17] and microbially active. Thus, the active layer is a potentially significant source of carbon into the atmosphere. The active layer also supports a productive vegetative community (dominated by black spruce trees, sphagnum moss, and grasses at the field sites discussed here). Thus, there is a balance between carbon fixing due to photosynthesis and carbon emission from microorganisms within the active layer. In the region of intermittent permafrost that is the focus of this paper, carbon sinking has outweighed carbon sourcing on an annual basis, but there has been a trend toward carbon sourcing over the last several summer seasons [18]. The primary motivation for the current study is the development of an instrument that can provide additional concentration data for carbon dioxide and methane at meaningful spatial and temporal resolution in the near-surface atmosphere where the interplay between photosynthesis and microbial activity will be most critically important.

Open-path spectroscopy to achieve spatially integrated trace-gas measurements via Fourier transform infrared (FTIR) spectroscopy or tunable diode laser absorption spectroscopy (TDLAS) has been reported [19–28]. The use of FTIRs, although providing the opportunity for broadband measurement at high spectral resolution, is not cost effective or practically feasible for measurements in remote locations. Wavelength or frequency modulation TDLAS techniques, despite having the potential to achieve relatively high sensitivities, require calibration, often with an inline reference material, under experimental conditions [29]. Some calibration-free wavelength modulation studies over modest optical path lengths have been conducted [30–32]. In addition, the use of chirped laser dispersion spectroscopy (CLaDS) in both the mid-infrared and near-infrared has been demonstrated [33–35]. CLaDS allows for resilience to intensity fluctuations in laser diodes, but also requires a real-time reference to be present with the instrument and utilizes RF electronics that can impose a significant power burden [33–35]. Further, the use of mid-infrared light may require less mature optical fiber technology (as compared to that used in the sensor described below) and typically the use of quantum cascade (QC) lasers that impose additional power needs. Direct TDLAS in the near-infrared allows for a more simplistic design utilizing low-cost, robust distributed feedback (DFB) laser diodes while achieving an essentially calibration-free measurement, but—as demonstrated here—lower absorption levels and thus degraded precision.

In this manuscript, we present the development of a relatively inexpensive, portable, open-path direct absorption tunable diode laser sensor for the measurement of trace-gas species above thawing permafrost in remote Alaska. While near simultaneous measurements of both CO_2 and CH_4 are the goal of this project, in this manuscript we only report on the former. As will be shown, this is a challenging problem for several reasons. First, line strengths for CO_2 at 1572 nm are weak compared to those for vibrational bands at longer wavelengths: a 200 m round trip path will only produce a 1% absorption. Second, under the best circumstances, maintaining alignment on a 50 mm diameter retroreflector at 55 m is challenging requiring a pointing accuracy of 0.05°. In this field site, this last factor is exasperated by large diurnal swings in temperature (from 5 to greater than 25°C) as well as unstable, water-saturated vegetation and active layers that compromise alignment. As will be shown, these issues limit the ultimate precision of the instrument deployed, but are sufficient to follow diurnal cycles for CO_2 in this environment.

2 Methods

Measurements were performed in the near-infrared (NIR) with a DFB laser centered near 1572 nm (NEL NLK-1LEAAA) for CO_2 detection. For direct absorption measurements, the laser was tuned 0.39 nm (1.58 cm^{-1}) by sweeping

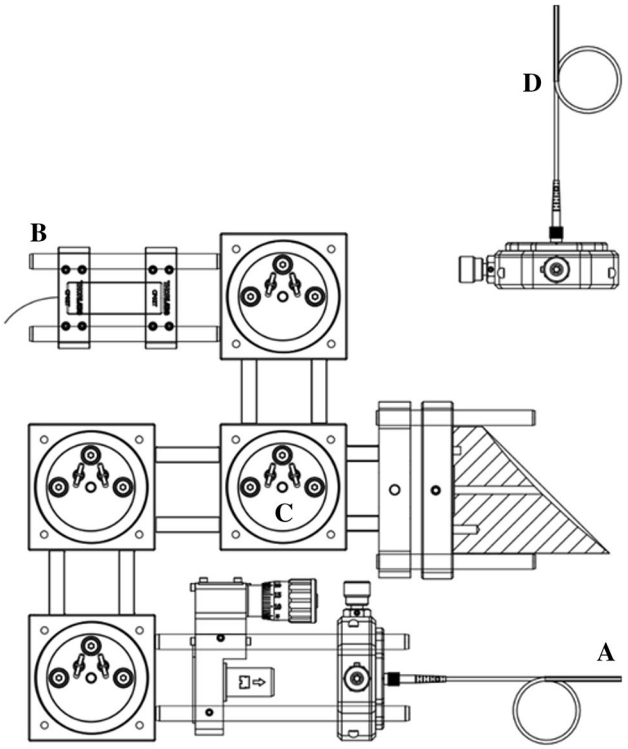

Fig. 1 Optics launch-box. Cage-mounted optics sit on a 30.5 cm square plate and are used to simultaneously send and receive laser light. The NIR laser is fiber-coupled into the system (**a**) and combined with a visible laser beam (**b**) using a dichroic mirror (**c**) before exiting through a 3.2-mm hole in the parabolic mirror. A retroreflector is placed downfield which returns the laser light to the launch-box where the beam is collected on the remainder of the parabolic surface and subsequently focused onto a 1-mm core multimode fiber (**d**) to be sent to an InGaAs detector (Thorlabs PDA10CF)

the injection current over 50 mA while keeping temperature stable. An Arduino Due was used as a waveform generator to supply a 200 mV, 500 Hz sawtooth ramp to a compact, combination laser diode driver and temperature controller with a transfer function of 250 mA/V (Wavelength Electronics LDTC0520, below referred to as "WEC"). The laser was fiber-coupled to the optics "launch-box", as shown in Fig. 1. The launch-box employs a two-channel design that co-aligns the visible laser beam in the upper channel with the near-infrared beam of the lower channel, using a long-pass dichroic mirror (DMLP1180), for alignment purposes.

In this work, we discuss two-system configurations. In the first, the launch-box is aligned with a Laser Analytics multi-pass White cell (model 5210) for measurement of a controlled concentration of CO_2. Experiments using the White cell did not utilize the collection portion of the optics box, but instead the laser light was collected directly onto a Thorlabs PDA10CF InGaAs detector after exiting the cell (Fig. 2). An Omega flow controller (FMA5510) was used to provide a constant flow of calibrated CO_2 gas, balanced with nitrogen (Praxair), to the White cell. The CO_2 tank was calibrated with a Los Gatos Research Ultraportable Greenhouse Gas Analyzer (UGGA). Temperature on the optical table was monitored with a thermometer as well as an integrated environmental sensor (Bosch BME280, ±1 °C) communicating with a raspberry pi microcontroller. Pressure in the cell was monitored via an Inficon pressure transducer (CDG150). Cell CO_2 concentrations were determined through spectral fitting using the known values of temperature, pressure within the cell, the cell pathlength, and after accounting for contributions to the absorption signal from the ambient laboratory air external to the cell (as described in more detail below).

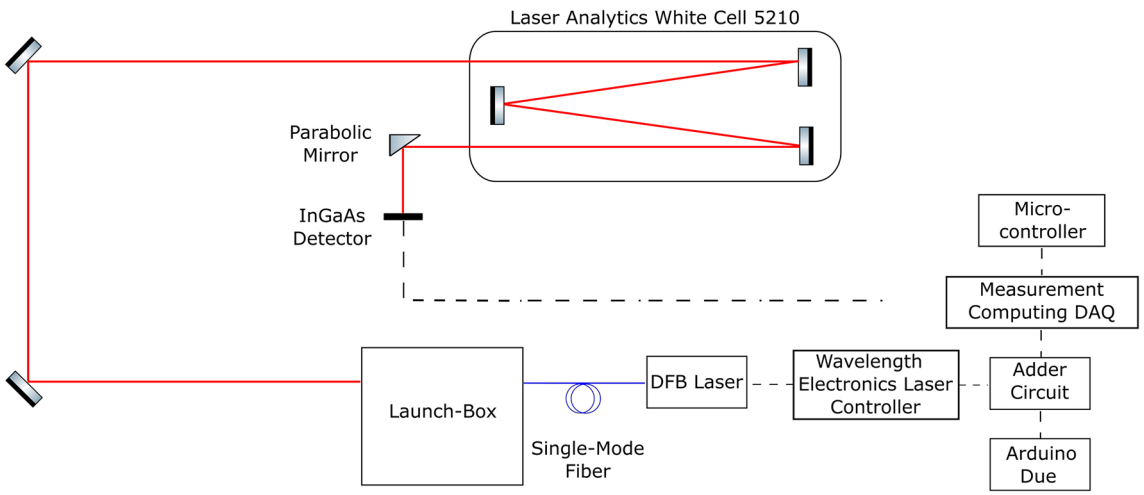

Fig. 2 Laboratory configuration of the open-path instrument aligned with a multipass White cell. This configuration was used for all measurements of nitrogen-balanced, calibrated CO_2 gas

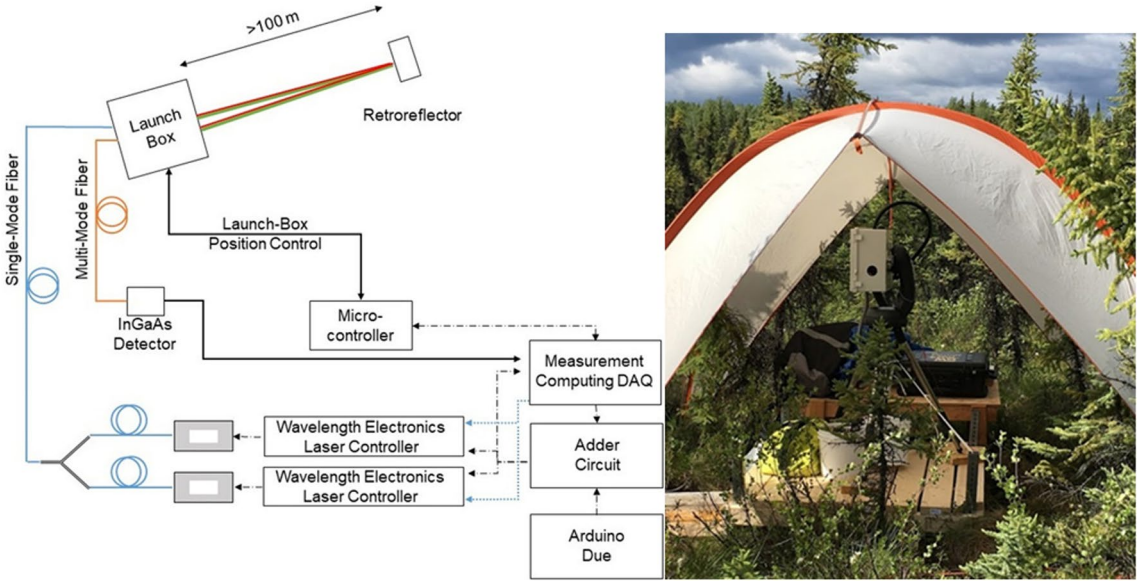

Fig. 3 Open-path instrument configuration for field measurements. The *block diagram* (*left*) shows analog communication required to monitor and ramp the laser diodes represented by the *black dashed lines* and digital communication used for rastering laser diodes is shown with the *blue dotted line*. An image of the instrument deployed in the field is shown in the photograph to the right. All the electronics are mounted onto a chassis that fits into the 56 × 35 × 23 cm case (*black*) shown in center frame connected via umbilical to the beige launch-box shown above and just to the *left* of the electronics case

In the second configuration, the launch-box is aligned with a retroreflector placed downfield for an open-path measurement (Fig. 3). Use of a retro-reflecting corner cube as opposed to inexpensive alternatives [22] was to maintain optimum collimation and co-linear return of the laser beam. In planning for the instrument deployment, the target distance was 100 m, or 200 m total pathlength, in an effort to achieve >1% absorption. However, the distance between the launch-box and retroreflector was constrained by measurement location and at this field site the maximum distance achieved was approximately 55 m or a total 110 m with return path. The spectral feature selected, the $R(16)$ line of the 30012 ← 00001 transition (using the AFGL notation [36]) centered at 1572.33 nm, has a line strength of 1.744×10^{-23} cm^{-1}/(molecule × cm^{-2}) [37].

In both configurations, a Measurement Computing (MCC), 16-bit data acquisition device (USB-1608GX-2AO) was used to record the detector's response to returned laser power. Using custom, precompiled DAQ ***c*** code, and driven by Python control scripts, the USB-1608GX-2AO was synced with the function generator and could collect 500 sweep-scans per second. All MCC device control and data logging were performed with an ARM processor-based microcontroller (Raspberry Pi 3 Model B) running a Debian Linux distribution. The total power burden of the instrument is approximately 18 W.

3 Spectral analysis

Experimental absorption spectra were fit using in-house spectral simulation software (SpecSyn) where the HITRAN 2008 database provides the spectral parameters required for simulations. As a first step in this analysis, a baseline fitting algorithm was applied to the raw signal, in voltage, collected from the InGaAs detector to account for the ~30% amplitude modulation from variation in injection current. For this, approximately ten baseline points on either side of the spectral feature were used to fit a third-order polynomial to obtain a value for I_0 across the tuning region. Detector "dark" voltage was checked daily and was found to be invariant. Absorbance was then calculated by taking the logarithm of the ratio of actual transmitted light intensity to the calculated I_0, both corrected for "dark" voltage. Data from a wavenumber calibration of the laser, performed with a Burleigh Wavemeter (WA-1000), were implemented to convert the laser temperature and injection current to emitted frequency. The latter was controlled by an analog input line on the MCC DAQ with a 250 mA/V transfer function. This experimental spectrum was then fit, using a simplex routine, to a simulated SpecSyn spectrum using a Voigt line profile based on known temperature, pressure, and optical pathlength. For all spectral simulations and fits discussed here, real-time temperature was obtained from an integrated

environmental sensor (Bosch BME280) communicating with a raspberry pi microcontroller with a manufacturer's accuracy of ±1 °C. As noted above, pressure measurements in the laboratory were made with an Inficon pressure transducer (CDG150), whereas in the field the Bosch sensor was employed, with an accuracy of ±1 mbar.

Direct absorption spectroscopy is often referred to as a calibration-free technique. This can be rationalized by considering the Bouguer–Lambert law which defines absorption signals as:

$$A = S(T) \cdot g(v, P, T) \cdot \rho(P, T) \cdot x_j \cdot l. \quad (1)$$

Four of the five parameters required to characterize an absorption signal in Eq. 1 are known quantities acquired from the HITRAN database (S (T): line strength); mathematically determined physical constants for the target molecule (g (ν, P, T): line shape factor, ρ: molecular density); or known experimental parameters (l optical path length, P pressure, T temperature). This leaves only concentration of the target molecule (x_j) as an unknown parameter to model and fit an experimental absorption feature. In the fitting procedure, a test spectrum is calculated assuming unit mixing ratio of the test molecule CO_2 at the temperature and pressure of the experiment (but assuming air-broadened collision parameters). This concentration (as well as slight wavelength and baseline dithers) is fit to minimize residuals between the calculated and observed spectra. The resulting model spectrum is interpolated to match the wavenumber values of the experimental spectrum before fitting.

An additional parameter was incorporated into the SpecSyn model for this work: a halfwidth factor (HWF) of 1.11 was multiplied by the air-broadened halfwidth reported in HITRAN and resulted in improved fit quality. The ideal HWF was determined by examining shape and magnitude of fit residuals under known experimental conditions, as depicted in Fig. 5. The rationale for the increased halfwidth might be related to uncertainty in the HITRAN broadening data. However, for this CO_2 line, both the GEISA and HITRAN databases agree on both the line strength and air-broadened collision width for this feature. Another, and more likely, cause may be traceable to laser temperature control. The typical short-term temperature stability of the WEC is reported as 0.002 °C. From our calibration data, this variation of temperature instability would shift an absorption line by 10% of the air-broadened halfwidth.

In the results reported below for instrument characterization in the laboratory, the absorption cell was filled with a mixture of CO_2 in N_2 that flowed from a tank whose concentration as reported by the distributor was 1013 ppm. This concentration was also measured using a Los Gatos Research Ultraportable Greenhouse Gas Analyzer that reported a concentration of 988 ppm with a ten second-measurement cycle. Corrections were made for ambient CO_2 contributions to the experimental absorbance signal with a measured pathlength of 235 cm and using the ambient CO_2 as monitored with a calibrated, non-dispersive infrared sensor (K30 from Senseair). This sensor has a manufacturer's specified accuracy of ±30 ppm ±3% of reading. However, after determining an offset value using a zero calibration procedure, we have found accuracy better than 1% for gas from a 393 ppm CO_2 in N_2 mixture (also calibrated against the LGR ICOS instrument). To determine concentrations from our own fits, the path length in the cell is required. This was determined by counting spots on the field mirror and calculating pathlength (in m) as:

$$l = 4.17 + \left[\frac{(n-1)}{2}\right] \cdot 4 \text{ m}, \quad (2)$$

where n is the numbers of spots; 19 in the results reported here, leading to a cell path length of 40.17 m.

Uncertainty in each spectral fit was evaluated through Monte Carlo methods. For each fit, the noise level of the experimental spectrum, standard deviation of the fit residuals, was applied onto a modeled version and then repeatedly fit for one-thousand consecutive trials. The standard deviation in reported concentration as a result of these fits was then propagated with the uncertainty in experimental path length to determine the overall fit uncertainty in parts per million (ppm).

For field measurements, a multi-species version of this fitting protocol is implemented. Following the same procedure as outlined above, a multi-species fit requires SpecSyn to simulate model spectra of all potential molecules present (CO_2, H_2O, and CH_4 in our case). The model spectrum for water was calculated using the mole fraction determined from the relative humidity (RH) and pressure measured by local BME280 sensors (±3% RH, ±1 mbar). Simulations were performed of CO_2 and CH_4 at unit concentration over the experimental frequency range, and then co-added with the water spectrum determined from the humidity sensor, and then fit to the experimental spectrum by adjusting their concentrations to minimize residuals.

4 Results

4.1 Allan–Werle analysis

To determine optimum data collection time, an Allan–Werle analysis [38] was performed and the resulting plot of Allan–Werle deviation as a function of averaging time was constructed. Data used for this analysis were collected with the experimental setup shown in Fig. 2. Single-sweep data files were collected over the course of 300 s and averaged at time intervals ranging from 1 to 100 s. For each time

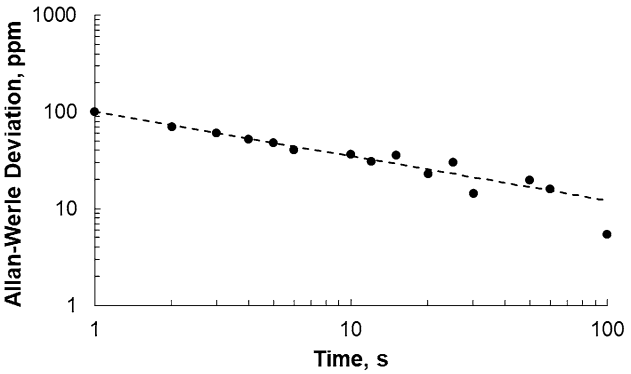

Fig. 4 Allan–Werle deviation plot for CO_2 reported concentration. The minimum deviation along the trendline is 5.4 ppm which corresponds to a 100 s time average. However, noise in the fit begins to increase after 10 s (Allan–Werle deviation = 36.9 ppm)

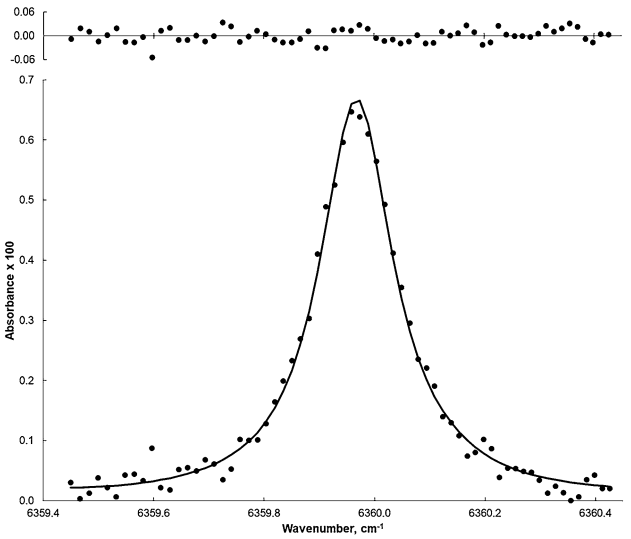

Fig. 5 Example spectrum for a 10 s time average is shown with corresponding fit residuals (*upper*)

interval, resulting absorbance spectra were fit according to the protocol detailed above and the Allan–Werle deviation of reported concentration within the dataset was determined. The log–log plot of this deviation as a function of time is shown in Fig. 4. The dashed trendline, with a slope of −0.458, shows a linear decrease in the Allan–Werle deviation across all averaging intervals with noise in the fit increasing somewhat after 10 s of averaging. 10 s was selected as the sampling time for all further studies based on this Allan–Werle analysis, as well as, consideration of environmental factors (such as fluctuation in temperature and ambient gas concentration) and their potential impact on measurements in the field. An example fit with residuals is shown in Fig. 5.

4.2 Reporting-interval averaging

A 2 h data record was obtained using 10 s sampling intervals (of 5000 sweeps each) in order to examine long-term drift of the instrument and the potential for reporting-interval averaging of data collected at relatively short single-sample time frames. Figure 6 shows reported fit concentrations as a function of time. More than 90% of the observed 10 s measurements fall within 36.9 ppm deviation from the average value as expected from the Allan–Werle deviation analysis. The average value (959.8 ppm) fell below the tank concentration of 988 ppm as determined by the LGR-UGGA).

Figure 7 shows results of averaging multiple 10 s absorbance files collected in the White cell configuration in an effort to determine an ideal reporting-interval. Datasets were constructed where 2–5000 sweep data files were averaged prior to fitting resulting spectra, another where 3–5000 sweep data files were averaged, and so on. Allan–Werle analysis was not performed here due to the presence of dead time in between samples as a result of averaging being done post-collection [30]. Instead, traditional standard deviation was employed. It is important to note that, in the field, averaging is done in real-time eliminating any overhead between measurements.

The motivation here was to ensure an appropriate averaging method was available for experimental scenarios with transient laser temperature conditions that would result in peak shifting. Averaging raw voltage under changing laser temperature conditions could introduce peak broadening if the center of the absorption feature is not located at the same ramp value in each data file. By converting each 10 s measurement to an absorbance spectrum and correcting for any shift in wavenumber prior to averaging, we can improve the precision of data collected by more than 85%. Standard deviation of the 10 s measurements was determined to be 22.1 ppm and deviation at 570 s (9.5 min), the maximum reporting interval before results deviated from linearity, was 3.0 ppm. This averaging technique was employed for all data collected in the field.

4.3 Example of data collected during deployment

The open-path instrument was deployed during June 2017 in the Bonanza Creek Long-Term Ecological Research Site near Fairbanks, Alaska. Instrument performance along with initial results from the field campaign has been evaluated. Measurements were made in a young bog with nearly 110 m round trip pathlength. Temperature and pressure were independently measured at the instrument's launch and midway between the launch and target using Bosch BME280 sensors communicating with raspberry pi microcontrollers, as discussed above. Based on line strength and global ambient

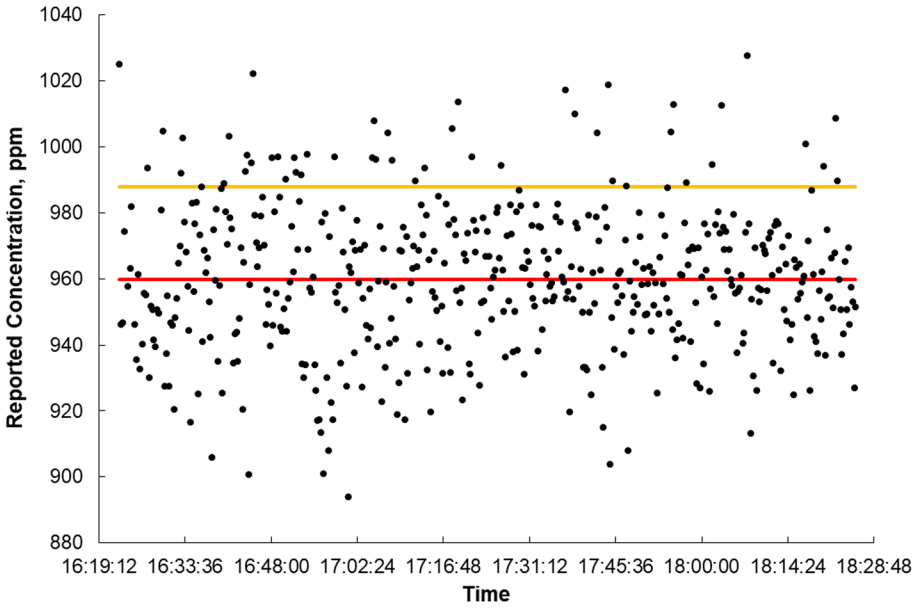

Fig. 6 Plot of reported CO_2 concentrations using a cell pathlength of 40.17 m over the course of 2 h. Data were collected at 10 s sampling intervals. Averaging of 10 s data was done post-collection introducing some overhead in between samples. The *orange horizontal line* shows the LGR-ICOS reported value of 988 ppm and the *red horizontal line* shows the determined average value for the 2 h measurement

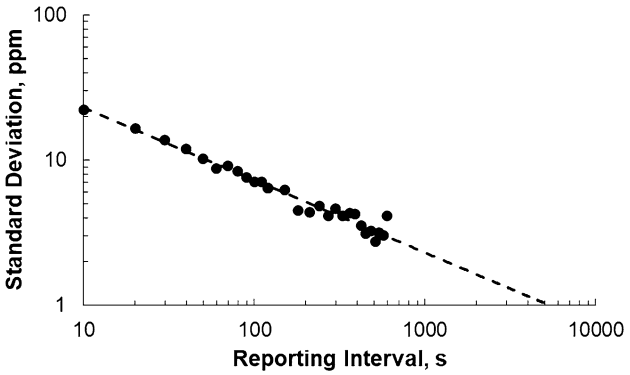

Fig. 7 Log–log plot of standard deviation in reported concentration as a function of reporting interval time. The *slope* of the *dashed trendline* is −0.498

concentrations of CO_2, the expected absorption signal was just over 0.5%.

Data collected in the field were deemed suitable for fitting if power to the instrument was maintained and returned laser signal was above a pre-determined threshold. The threshold is determined using the bit resolution of the digitizer and expected fractional absorption of ambient CO_2. A 16-bit digitizer with adjustable gain was employed allowing for increased sensitivity. Gain settings were selected based on return signal observed by the detector. At the bog site, a ±5 V gain setting was used. Knowing that we need to resolve absorption signals as low as 0.5%, the minimum return signal could be no less than 91.6 mV for a signal-to-noise ratio (SNR) of 3.

The primary factor contributing to limitations in return signal was ground sensitivity at the field site. The surface of the bog, composed primarily of sphagnum moss, was interconnected such that movement within a few feet of the instrument would result in tilting of the launch-box leading to misalignment. Preventative measures included the construction of an approximately 1.5 m^2 deck which was suspended above the surface (seen in Fig. 3). This deck reduced sensitivity to localized movement, but alignment was still impacted by ground changes as a result of large-magnitude temperature change (as great as 25 °C was observed) throughout the day.

Figure 8 shows an excerpt of a diurnal cycle seen at the young bog site in 2017. Data shown here from the open-path sensor (red diamonds) are 10 s measurements averaged to reporting intervals of 2.5 min. Intermittent gaps are due to CH_4 and CO_2 data that are yet to be analyzed. As discussed in the "Spectral Analysis" section of this manuscript, corrections for spectral interferences from additional species were implemented in fitting. Presently, the expected mole fraction of water is calculated from relative humidity and pressure measurements and integrated into the spectral fitting protocol. Fitting accuracy was tested by simulating the presence of ambient CO_2 (400 ppmV) with a range of H_2O concentrations (0.5–2%). If the mole fraction of water is known, concentration determination is accurate within <1 ppm.

Temperature and pressure used in each fit were concurrent 2.5 min averages observed by the BME280 at the instrument's launch allowing fit parameters to accurately reflect changing conditions at the field site. The mid-range sensor data were not used here due to influence from solar radiation on enclosure temperature during daylight hours which will be corrected for in subsequent analyses. Accurate temperature and pressure measurements along the lasers path are imperative for an accurate measurement. Using line strengths from HITRAN, we can expect an uncertainty of approximately 1 ppm per

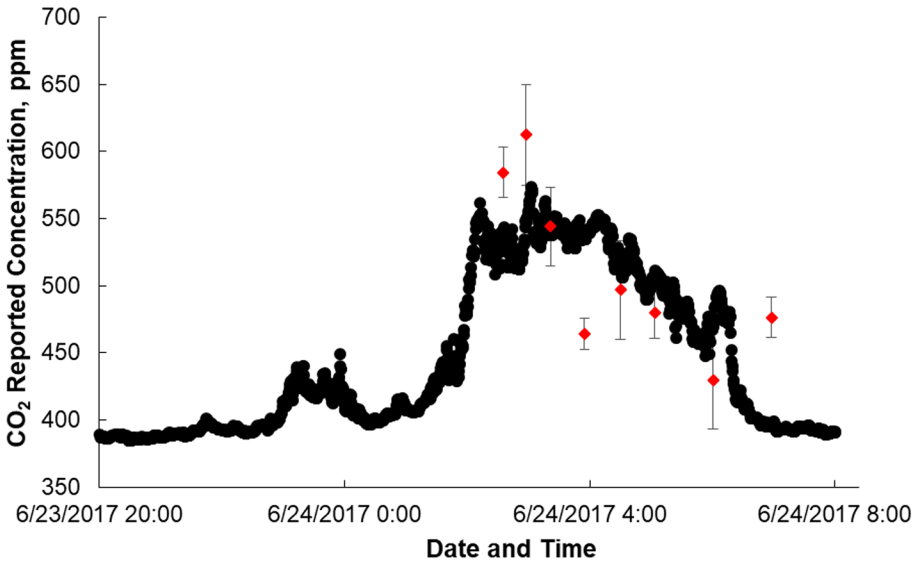

Fig. 8 12-hour excerpt of a diurnal cycle at the young bog site. Data shown here were collected from the evening of June 23, 2017 through the morning of June 24, 2017. NDIR data (*black*) collected at the laser instrument's launch are shown at 30 s sampling intervals. Open-path data (*red*) are 2.5 min averages with error bars corresponding to spectral fit uncertainty

degree temperature change. While lower sensitivity is seen for pressure uncertainty, 0.02 ppm per mbar, neither effect can be overlooked in our analysis. These data show a diurnal trend observed in other sensors at the field site (including our NDIR sensors) in which daytime CO_2 levels remain relatively low near 400 ppmV with early morning increases to 500 ppmV or higher, possibly traceable to decreased photosynthesis and breakthrough of CO_2 from the active layer.

The 2.5-min sampling interval was selected due to the changing CO_2 conditions at the field site and the expected precision of the instrument. Figure 9 shows standard deviation in concentration from a calibrated NDIR sensor, measuring localized CO_2 levels at the open-path instrument's launch, at 2.5 and 9.5-min intervals. These data show that ~45% of the time, when averaged at 9.5 min, concentration variation will be less than the instrument precision. When averaging at 2.5 min, expected CO_2 concentrations vary less than the expected instrument deviation 89% of the time. Therefore, 2.5-min time averages allow us to capture a clearer understanding of the changes in CO_2 concentration. Observed noise levels in the field were substantially higher than those observed in the laboratory, thus limiting SNR to levels less than 38 in most cases due to several environmental factors including wind movement of retroreflector and laser temperature stability.

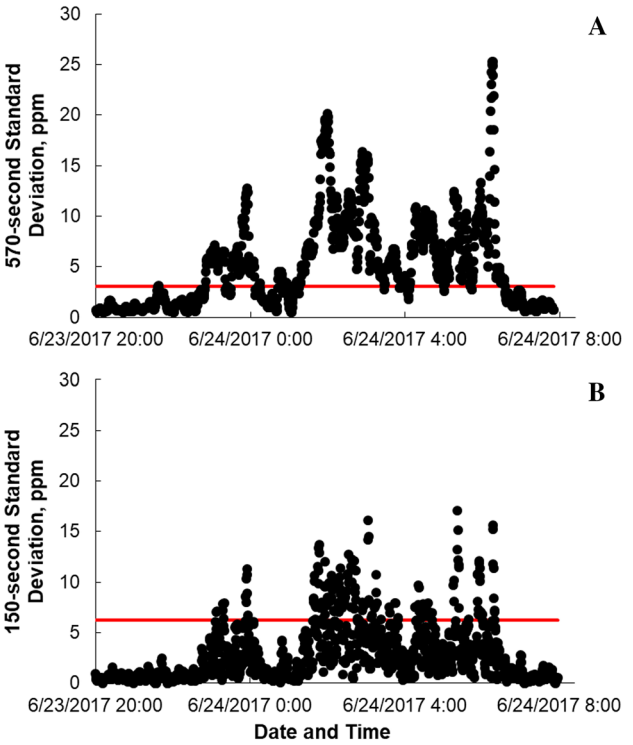

Fig. 9 Data collected from a local NDIR sensor were used to determine averaging intervals for open-path measurements. 570 s intervals (**a**) would overlook significant changes in CO_2 concentrations since standard deviation of measurements from the NDIR sensor was greater than the open-path instrument precision (*red line*) nearly 56% of the time. Choosing a 150 s average allows for finer changes in CO_2 concentrations to be observed

5 Discussion

Here, we have demonstrated the development and initial deployment of an open-path tunable diode laser sensor deployed near Fairbanks, Alaska for the detection of CO_2 above thawing permafrost. In its current configuration, the instrument has a power burden of approximately 18 W. The launch-box portion of the design readily accepts other NIR

fiber-coupled lasers for measurement of additional molecules, such as CH_4, while the electronics design allows for rastering between laser diodes through digital signals. Data are collected at a rate of 500 sweeps per second.

Characterization of the instrument showed single-measurement collection times up to 300 s, limited by the memory of the raspberry pi computer, can be used in a laboratory setting to obtain precision near 5.4 ppm with 100 s averaging. For practical measurements in the field, we selected a single-measurement time of 10 s in an effort to minimize the impact of changing environmental factors on data quality. To improve upon the precision of the 10 s measurement, we showed that reporting-interval averaging can be implemented up to 9.5 min to reduce deviation further to 3.0 ppm. This allows us to minimize effects on single measurements and respond to changes induced by temperature drift of the laser or environmental conditions at the field site.

It is important to note the limitations associated with the measurement configuration used for collection of Allan–Werle deviation and long-term laboratory data. First, the maximum pathlength that could be reached in the White cell, with certainty, was 40.17 m. Although the concentration of CO_2 flowed into the cell produced absorption signals on the same order as expected field concentrations, the ability to explore longer path lengths in the laboratory would be beneficial. Also limited by the White cell configuration is the laser return power. In the White cell, return signal from the detector was no larger than 1 V. However, in field measurements with longer path lengths, signals greater than 2 V were achieved. This increase in laser power directly impacts the digitizer's ability to resolve fine changes in absorption signal and leads to the argument that measurement deviation may be less than experimentally determined if noise levels are equivalent.

Initial field results indicate significant changes in CO_2 concentration throughout the day emphasizing the critical nature of continuous data collection with minimal loss due to decreases in returned laser power to correlate CO_2 behavior with seasonal conditions such as temperature and sun exposure. We are pursuing automatic optimization of laser alignment, using a Simplex method, to increase the overall up-time of the instrument as well as the amount of data with maximum returned laser power. Additional noise reduction techniques, such as the use of a Savitsky-Golay [39] filter for field data and potential redesign of the retroreflecting target for increased stability, are also being investigated along with the removal of the multimode fiber. By placing the InGaAs detector inside the optics box, we may increase overall return signal and remove any modal noise created by the multimode fiber.

This instrument was designed specifically for deployment in remote permafrost-containing areas to measure diurnal concentrations of CO_2. For this application, a precision of 3.0 ppm would be satisfactory when considering diurnal magnitudes near 100 ppm or more. As noted above, field environmental conditions compromised that goal. However, if increased precision is required a laser diode centered near 2051 nm could be implemented for CO_2 detection. The selected feature, the $R(30)$ line of the $20013 \leftarrow 00001$ transition, centered at 2050.97 nm, has a linestrength of 1.504×10^{-22} $cm^{-1}/(molecule \times cm^{-2})$ [37] which under field conditions leads to absorption signals of nearly 8% at 400 ppmV CO_2, an order of magnitude greater than observed with the 1572 nm diode. As a result, the digitizer's ability to resolve fine changes in fractional absorption will significantly improve. For example, based on the maximum averaging time determined in Fig. 7, the minimum-observable change in CO_2 absorption signal is currently 3.0 ppm. This corresponds to a fractional absorbance of 2.5×10^{-3}, similar to the results reported by others for open-path measurements [22], but larger than the minimum detectable absorption via direct TDLAS without implementing modulation techniques [40, 41]. Assuming we achieve the same fractional absorption, the use of the 2051 nm diode has the potential to drive our instrument sensitivity down an order of magnitude. Integration of the 2051 nm diode would require no change to the electronics design and minimal adjustment to the optics for a significant impact on overall sensitivity.

Acknowledgements Funding for this project is provided by the NASA Hydrospheric and Biospheric Science Research Program (Grant/Cooperative Agreement Number NNX14AN89G). The authors would like to thank our collaboration partners led by Dr. Emily L. Wilson (NASA Goddard) and Dr. Eugenie Euskirchen (University of Alaska—Fairbanks). We would also like to thank Prof. Amy Zanne for the loan of the LGR sensor used in calibration procedures.

References

1. IPCC, 2014: Climate Change 2014: Synthesis Report. Contribution of Working Groups I, II and III to the Fifth Assessment Report of the Intergovernmental Panel on Climate Change [Core Writing Team, R.K. Pachauri and L.A. Meyer (eds.)]. IPCC, Geneva, Switzerland (2014)
2. IPCC, 2007: Climate Change 2007: Synthesis Report. Contribution of Working Groups I, II and III to the Fourth Assessment Report of the Intergovernmental Panel on Climate Change [Core Writing Team, Pachauri, R.K and Reisinger, A. (eds.)]. IPCC, Geneva, Switzerland (2007)
3. UNFCCC. Conference of the Parties (COP), United Nations Office at Geneva, Geneva, Switzerland (2010)
4. T. Yokota, Y. Yoshida, N. Eguchi, Y. Ota, T. Tanaka, H. Watanabe, S. Maksyutov, SOLA **5** (2009)
5. T.E. Taylor, C.W. O'Dell, C. Frankenberg, P.T. Partain, H.Q. Cronk, A. Savtchenko, R.R. Nelson, E.J. Rosenthal, A.Y. Chang, B. Fisher, G.B. Osterman, R.H. Pollock, D. Crisp, A. Eldering, M.R. Gunson, Atmos. Meas. Technol. **9**, 3 (2016)
6. D. Crisp, H.R. Pollock, R. Rosenberg, L. Chapsky, R.A.M. Lee, F.A. Oyafuso, C. Frankenberg, C.W. O'Dell, C.J. Bruegge, G.B. Doran, A. Eldering, B.M. Fisher, D. Fu, M.R. Gunson, L.

Mandrake, G.B. Osterman, F.M. Schwandner, K. Sun, T.E. Taylor, P.O. Wennberg, D. Wunch, Atmos. Meas. Technol. **10**, 1 (2017)
7. M. Inoue, I. Morino, O. Uchino, Y. Miyamoto, Y. Yoshida, T. Yokota, T. Machida, Y. Sawa, H. Matsueda, C. Sweeney, P.P. Tans, A.E. Andrews, S.C. Biraud, T. Tanaka, S. Kawakami, P.K. Patra, Atmos. Chem. Phys. **13**, 19 (2013)
8. M. Zhou, B. Dils, P. Wang, R. Detmers, Y. Yoshida, C.W. O'Dell, D.G. Feist, V.A. Velazco, M. Schneider, M. De Mazière, Atmos. Meas. Technol. **9**, 3 (2016)
9. D. Wunch, G.C. Toon, J.F. Blavier, R.A. Washenfelder, J. Notholt, B.J. Connor, D.W. Griffith, V. Sherlock, P.O. Wennberg, Philos. Trans. R. Soc. A **369**, 1943 (2011)
10. Y. Miyamoto, M. Inoue, I. Morino, O. Uchino, T. Yokota, T. Machida, Y. Sawa, H. Matsueda, C. Sweeney, P.P. Tans, A.E. Andrews, P.K. Patra, Atmos. Chem. Phys. **13**, 10 (2013)
11. S.S. Kulawik, J.R. Worden, S.C. Wofsy, S.C. Biraud, R. Nassar, D.B.A. Jones, E.T. Olsen, R. Jimenez, S. Park, G.W. Santoni, B.C. Daube, J.V. Pittman, B.B. Stephens, E.A. Kort, G.B. Osterman, Atmos. Chem. Phys. **13**, 6 (2013)
12. S.C. Wofsy, H.S. Team, M. Cooperating, T. Satellite, Philos. Trans. R. Soc. A **369**, 1943 (2011)
13. P. Farrell, D. Culling, I. Leifer, Atmos. Environ. **74** (2013)
14. C. Schadel, M.K.F. Bader, E.A.G. Schuur, C. Biasi, R. Bracho, P. Capek, S. De Baets, K. Diakova, J. Ernakovich, C. Estop-Aragones, D.E. Graham, I.P. Hartley, C.M. Iversen, E. Kane, C. Knoblauch, M. Lupascu, P.J. Martikainen, S.M. Natali, R.J. Norby, J.A. O'Donnell, T.R. Chowdhury, H. Santruckova, G. Shaver, V.L. Sloan, C.C. Treat, M.R. Turetsky, M.P. Waldrop, K.P. Wickland, Nautre Clim. Change **6**, 10 (2016)
15. J.K. Jansson, N. Tas, Nature Rev. Microbiol. **12**, 6 (2014)
16. W.F. Vincent, M. Lemay, M. Allard, Arctic Science **3**, 2 (2017)
17. K.C. Kelsey, K.P. Wickland, R.G. Striegl, J.C. Neff, Arc. Antarc. Alp. Res. **44**, 4 (2012)
18. E.S. Euskirchen, C.W. Edgar, M.R. Turetsky, M.P. Waldrop, J.W. Harden, J. Geophys. Res. Biogeosci. **119**, 8 (2014)
19. T. Fernholz, H. Teichert, V. Ebert, Appl. Phys. B **75**, 2–3 (2002)
20. B. Kühnreich, S. Wagner, J.C. Habig, O. Möhler, H. Saathoff, V. Ebert, Appl. Phys. B **119**, 1 (2015)
21. A. Seidel, S. Wagner, A. Dreizler, V. Ebert, Atmos. Meas. Technol. **8**, 5 (2015)
22. A. Seidel, S. Wagner, V. Ebert, Appl. Phys. B **109**, 3 (2012)
23. T.K. Flesch, R.L. Desjardins, D. Worth, Biomass Bioenergy **35**, 9 (2011)
24. E.D. Thoma, R.C. Shores, E.L. Thompson, D.B. Harris, S.A. Thorneloe, R.M. Varma, R.A. Hashmonay, M.T. Modrak, D.F. Natschke, H.A. Gamble, J. Air Waste Manag. Assoc. **55**, 5 (2005)
25. D. Griffith, D. Pohler, S. Schmidt, S. Hammer, S. Vardag, I. Levin, U. Platt, Geophysical Research Abstracts, **17**, EGU 2015-11449-3, (2015)
26. J. Rentz Dupuis, D.J. Mansur, R.M. Vaillancourt, D.L. Carlson, T. Evans, E. Schundler, L. Todd, K. Mottus, in *Imaging open-path Fourier transform infrared spectrometer for 3D cloud profiling* ed. by A.W. Fountain III, P. J. Gardner. Proc. SPIE 7304, Chemical, Biological, Radiological, Nuclear, and Explosives (CBRNE) Sensing X, 7304 0P. Orlando, Florida, United States 14–16 April 2009 (2009)
27. J.H. Rentz, J.R. Engel, D.L. Carlson, D.J. Mansur, R.M. Vaillancourt, G.J. Genetti, P. Griffiths, H. Yang, Proc. SPIE 5272, Industrial and Highway Sensors Technology (2004)
28. H. Xia, W. Liu, Y. Zhang, R. Kan, M. Wang, Y. He, Y. Cui, J. Ruan, H. Geng, Chin. Opt. Lett. **6**, 6 (2008)
29. A.P.M. Michel, D.J. Miller, K. Sun, L. Tao, L. Stanton, M.A. Zondlo, J. Atmos. Ocean Technol. **33**, 11 (2016)
30. G.B. Rieker, J.B. Jeffries, R.K. Hanson, Appl. Opt. **48**, 29 (2009)
31. X. Chao, J.B. Jeffries, R.K. Hanson, Appl. Phys. B **106**, 4 (2011)
32. K. Sun, X. Chao, R. Sur, C.S. Goldenstein, J.B. Jeffries, R.K. Hanson, Meas. Sci. Technol. **24**, 12 (2013)
33. M. Nikodem, G. Wysocki, Sensors **12**, 12 (2012)
34. M. Nikodem, G. Plant, D. Sonnenfroh, G. Wysocki, App. Phys. B **119**, 1 (2014)
35. G. Plant, M. Nikodem, P. Mulhall, R.K. Varner, D. Sonnenfroh, G. Wysocki, Sensors **15**, 9 (2015)
36. L.S. Rothman, L.D.G. Young, J. Quant. Spectrosc. Radiat. Transf **25**, 6 (1981)
37. L.S. Rothman, I.E. Gordon, A. Barbe, D.C. Benner, P.F. Bernath, M. Birk, V. Boudon, L.R. Brown, A. Campargue, J.P. Champion, K. Chance, L.H. Coudert, V. Dana, V.M. Devi, S. Fally, J.M. Flaud, R.R. Gamache, A. Goldman, D. Jacquemart, I. Kleiner, N. Lacome, W.J. Lafferty, J.Y. Mandin, S.T. Massie, S.N. Mikhailenko, C.E. Miller, N. Moazzen-Ahmadi, O.V. Naumenko, A.V. Nikitin, J. Orphal, V.I. Perevalov, A. Perrin, A. Predoi-Cross, C.P. Rinsland, M. Rotger, M. Šimečková, M.A.H. Smith, K. Sung, S.A. Tashkun, J. Tennyson, R.A. Toth, A.C. Vandaele, J. Vander Auwera, J. Quant. Spectrosc. Radiat. Transf. **110**, 9–10 (2009)
38. P. Werle, R. Miicke, F. Slemr, Appl. Phys. B **57**, 2 (1993)
39. A. Savitzky, M.J.E. Golay, Anal. Chem. **36**, 8 (1964)
40. D.E. Heard, *Analytical Techniques for Atmospheric Measurement* (Blackwell Publishing Ltd, Oxford, 2006)
41. P. Werle, Spectrochim. Acta A **54**, 2 (1998)